The Journal of Experimental Biology 203, 2945–2955 (2000)
Printed in Great Britain © The Company of Biologists Limited 2000
JEB2911

THE HIND WING OF THE DESERT LOCUST (*SCHISTOCERCA GREGARIA* FORSKÅL)

III. A FINITE ELEMENT ANALYSIS OF A DEPLOYABLE STRUCTURE

R. C. HERBERT[1], P. G. YOUNG[2], C. W. SMITH[2], R. J. WOOTTON[1,*] AND K. E. EVANS[2]

[1]*School of Biological Sciences, University of Exeter, Hatherly Laboratories, Prince of Wales Road, Exeter EX4 4PS, UK* and [2]*School of Engineering and Computer Science, University of Exeter, Exeter EX4 4QF, UK*

*Author for correspondence (e-mail: r.j.wootton@exeter.ac.uk)

Accepted 29 June; published on WWW 7 September 2000

Summary

Finite element analysis is used to model the automatic cambering of the locust hind wing during promotion: the umbrella effect. It was found that the model required a high degree of sophistication before replicating the deformations found *in vivo*. The model has been validated using experimental data and the deformations recorded both *in vivo* and *ex vivo*. It predicts that even slight modifications to the geometrical description used can lead to significant changes in the deformations observed in the anal fan. The model agrees with experimental data and produces deformations very close to those seen in free-flying locusts. The validated model may be used to investigate the varying geometries found in orthopteran anal fans and the stresses found throughout the wing when loaded.

Key words: locust, *Schistocerca gregaria*, umbrella effect, functional biology, finite element modelling, insect flight, smart structure.

Introduction

Desert locusts obtain the majority of their thrust and weight support from the downstroke of their hind wings (Jensen, 1956; Cloupeau et al., 1979; Wootton et al., 2000). A particular feature of the downstroke is the automatic development of depression and camber by the promotion of the wing and the resulting deployment of the anal fan (‘vannus’ of Snodgrass, 1935): the so-called umbrella effect (Wootton, 1995). This serves to depress and hold the low-stiffness trailing edge, almost certainly improving aerodynamic efficiency (Wootton, 1995). The umbrella effect is one of a number of mechanisms that have been identified as controlling, either automatically or semi-automatically, the instantaneous three-dimensional shape of insect wings during flight (Wootton, 1992).

The muscles of the wing do not extend beyond the axillae, and no control input is required to generate the desired effect in the anal fan. The deformation is therefore encoded in the wing design, and the fan, short of catastrophic failure, will always adopt the same shape for a given angle of promotion. Although the wing incorporates some of the features associated with ‘smart’ structures, it is not truly a smart structure. Smart structures and materials have obvious attractions for engineers who wish to reduce the controlling component of small-scale machines and deployment mechanisms. This level of integration of design and function between and within biological structures is often far greater than that achieved by modern engineering.

Wootton (1995) has demonstrated that the process of automatic depression that leads to camber generation, referred to as the ‘umbrella effect’, is dependent on the wing’s geometry: the progressively decreasing length of the supporting veins postero-proximally from the remigium to the inner margin, and the acute angle that each makes with the perimeter. He derived an analytical model of the effect, which is also relevant to other Orthoptera and to some Phasmida (stick-insects) and Dictyoptera (cockroaches and mantises). He showed that, for a given angle of deployment, the height of the generated camber is inversely related both to the number of vannal veins and to the size of the acute angle between the veins and the perimeter. However, the model he used was based on a number of simplifying assumptions: the profile was described as part of a logarithmic (equi-angular) spiral; the perimeter was modelled as a cord, stiff in tension; and the wing membrane, cross-veins and intercalary veins were disregarded. In addition, the supporting veins were assumed to be straight and to radiate from a single point, and the flexural rigidity was assumed to be constant along the length of each vein and identical from vein to vein. In reality, the wing profile can only approximately be described as a logarithmic spiral, and the supporting veins radiate not from the same point but from a cuticular bar. The veins are curved, taper from their origin at the ano-jugal bar to their ends at the wing margin and, therefore, have non-constant flexural rigidities along their length. The limitations of the analytical model were discussed by Wootton (1995). However, to explore in detail the influence of these complicating effects, a more complex and realistic model is needed.

In the present paper, a finite element model of part of the desert locust wing is developed to explore numerically the mechanisms that lead to the umbrella effect. The finite element method was first introduced by Courant (1943) and developed further by physicists and engineers (Argyris, 1965). The impetus for development since has come from engineers who wished to gain solutions to many problems of complex continua in solid mechanics, fluid dynamics and shape optimisation. The finite element approach involves dividing a complex structure into simpler constituent elements that are connected to one another at common points or nodes, a process known as meshing. Specifically, it involves interpolating a field quantity, e.g. stress, displacement or temperature, at the nodes that are created when the model is meshed. By connecting the elements at the nodes, the field quantity becomes interpolated over the entire structure. Although the solution obtained is, in general, approximate, the strength of the approach lies in its versatility: structures can be of any shape, have any support conditions and be subjected to complex and multiple loads.

The non-linearity of biological systems, the structural and physical diversity of biological materials, the problems associated with their testing and the irregularity and complexity of structural components all present major problems for finite element modelling. The potential applications in biology are nonetheless numerous. The method has already been utilised extensively in biomedical physics, particularly for bone, whose material properties are relatively well understood (Huiskes and Chao, 1983; Prendergast and Huiskes 1996a,b; Prendergast, 1997; Smith et al., 1997; Hirschberg et al., 1999). The advent of accurate scanning techniques such as computer tomography has allowed meshing of complex and inhomogeneous three-dimensional structures of the sort commonly encountered in biology to be accurately modelled (Dalstra et al., 1995; Guldberg et al., 1998).

The finite element method has previously been used to model the wings of dragonflies (Odonata) (Kesel et al., 1998; Watanabe, 1995). These are perhaps the most complex of all insect wings, with high, varying relief and a rich network of multi-branched longitudinal veins and multiple cross-veins. Because of this complexity, and since the material properties of the cuticle and the actual spatial and temporal distribution of aerodynamic forces on dragonfly wings are unknown, the models have necessarily included simplifications. In both cases, the Young's modulus of all cuticle was taken from published values for the locust tibia (Jensen and Weis-Fogh, 1962). The models of Kesel et al. (1998) introduced complexity progressively, achieving increased realism in computed deformations in response to notional aerodynamic loads. However, many simplifications inevitably remained: the irregular, variable-cross-section veins were modelled as hollow cylinders, and the effect of the membrane was approximated by adding a stress-stiffening component. The sophisticated analysis of Watanabe (1995) incorporated precisely measured relief and membrane thickness, and subjected the modelled wings to computed inertial forces and aerodynamic pressures based on real dragonfly kinematics. The model was used to compare the stresses on the wings in which attitude and spanwise torsion were actively as well as aeroelastically controlled with those that would result when these were controlled by wing elasticity alone. The geometry of the veins was modelled as precisely as possible, but no account was taken of flexion lines or flexible joints, which probably contribute significantly to the deformations of the wings.

The current analysis will combine accurate material and geometric properties, obtained from direct measurement, to produce a robust numerical model of the umbrella effect in the hind wing anal fan of *Schistocerca gregaria*. It will ascertain the importance of certain features (vein geometries and position, wing shape) to the umbrella effect. The model will be validated using experimental camber tests and by comparing deformations with those observed *in vivo*.

Materials and methods

Vein geometry

The form of the cross sections of the longitudinal veins replicated in the models (Fig. 1) was found by sectioning. The veins were embedded in LR White, a two-part acrylic resin. The nature of insect cuticle makes it exceptionally difficult to achieve any real infiltration using embedding media. This results in poor sectioning where the material is unsupported, and distortions can occur if a microtome is used to cut thin sections. To prevent this, thick sections were cut manually. A metal guide was clamped either side of the sample, parallel to the vein's long axis, and the section was ground down until the guide was reached. This produced a clean, flat section perpendicular to the vein's long axis.

Each section was positioned under an Olympus microscope, fitted with a video-capture system. A small spirit level was used to ensure that the section was perpendicular to the objective. Images of the vein were captured, and the contrast was digitally enhanced if necessary. The width and height of the sample were measured. The use of perpendicular metal guides when cutting the samples and the spirit level when mounting the samples ensured that parallax errors were negligible.

To simulate numerically the structural behaviour of the locust wing in the finite element model, the flexural rigidity to be used in the beam elements modelling the veins is needed. The flexural rigidity of any beam is the product of its Young's modulus (E) and the second moment of area (I) of its cross section about the neutral axis. The second moment of area is the sum of the products of areas and the squares of their perpendicular distances from the neutral axis (Fig. 2). The neutral axis passes through the centroid of the section and is an imaginary line along which tensile and compressive stresses are zero when the beam is subjected to pure bending (Fig. 2). The Young's modulus is a uni-axial measure of stiffness given by the ratio of stress to strain in a material. Pictures taken from the sectioned veins were edited as bitmaps

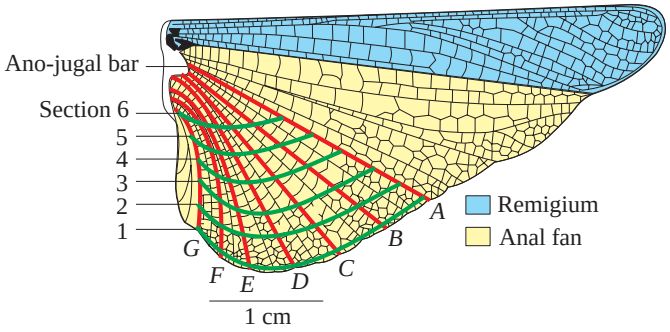

Fig. 1. A locust hind wing illustrating the extent of the anal fan (yellow) and the remigium (blue). The veins replicated in the model (*A*–*G*) are shown in red. The green intersecting lines indicate the points along the veins where sections were taken.

to isolate the vein material from the background and to convert the images to monochrome (Fig. 3). A program was designed that processes a shape image and calculates the cross-sectional area and all required area moments. These are I_{xx} and I_{yy} (the second moments of area of the section relative to bending forces from two directions mutually at right angles) and the torsional constant I_{xy}, an area moment that is a function of the resistance of the beam to torsion. The calculations were checked using regular shapes whose area moments were calculated using standard formulae (Young, 1989); the resulting error was 0.6 ± 0.3 % (mean ± S.D.). Preserving the shape of the veins during sectioning was of paramount importance, as any distortion would introduce critical errors in these calculations.

Wing geometry

A digitised wing profile was built up using drawings and photographs (Fig. 1). The coordinates of the wing structures were recorded and registered using a bitmap editor. Each vein was excised, and the profile of the *z* axis was recorded (along the vein, Fig. 4). The gross wing geometry was then entered as a set of *x*, *y* and *z* coordinates.

Experimental tests

The torques required to induce a 1 cm depression in the anal fan of the hind wings were measured using a torsion balance (Fig. 5) modified from that used by Wootton (1993). An adult locust (*Schistocerca gregaria* Forskål) was killed, the fore wings and legs were removed, and the flight muscles were severed. A small hole was made through the wing membrane behind the leading edge vein at a point that had previously been hardened with a small droplet of cyanoacrylate glue to prevent tearing. The hole was made 15 mm from the point of rotation about the wing base, matching the length of the moment arm on the torsion balance. The insect was mounted on a stage with the axilla lying co-axially to a vertically suspended metal wire of known length, diameter and torsional stiffness through which torque was applied (Fig. 5).

The lower end of the metal wire was glued to a needle that formed a vertical axle for an aluminium disc mounted on effectively frictionless bearings. A rod and hook projected from the underside of the disc, 15 mm from the centre point. The disc carried a horizontal pointer that moved around a horizontal circular protractor mounted co-axially with the wire, the disc and the axilla. The upper end of the wire was attached to a cork mounting, with a second pointer moving around a second horizontal, circular, co-axially-mounted protractor. Torque was applied manually by rotating the cork mounting, so rotating the aluminium disc and extending the wing. The torque applied to the wing was calculated by converting the difference in rotation angle between the top and bottom pointers into radians. This value was multiplied by the torsional rigidity of the wire (in $N\,m\,rad^{-1}$) to give the torque in N m. The total force applied at 15 mm from the base could then be calculated by dividing the calculated torque by 0.015 m.

Right and left hindwing pairs were tested 11 times each, disregarding the first test. Desiccation of the wing was minimised by maintaining a high ambient humidity with damp tissues and by carrying out the tests in less than 2 min. Each time torque was applied, the leading edge was promoted and

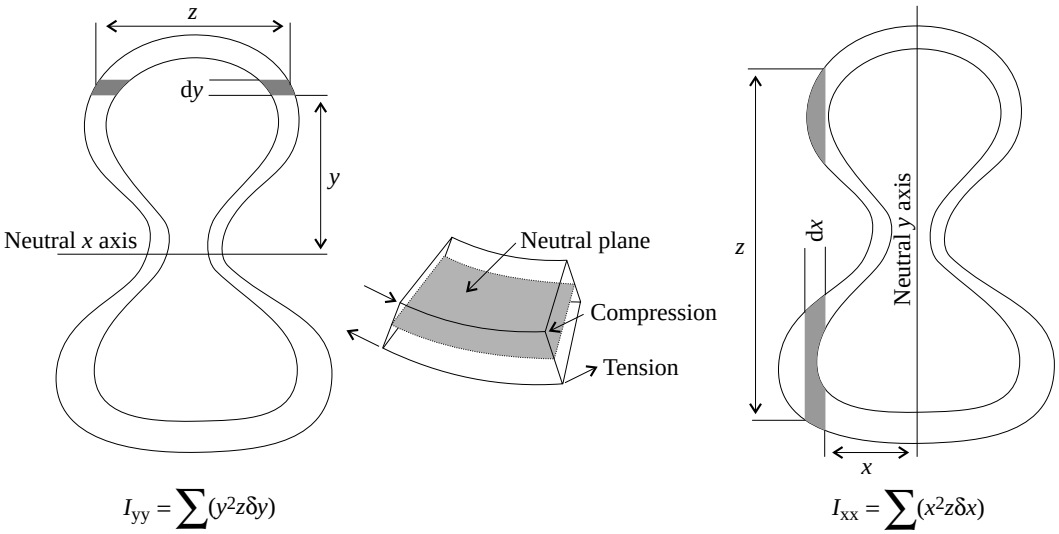

Fig. 2. Calculation of the second moments of area I_{yy} and I_{xx} of a section of a tubular vein, respectively, about the neutral *x* and *y* axes. The neutral axis is a section of a plane where the stresses due to bending are zero (inset). I_{xx} and I_{yy} are moments of area.

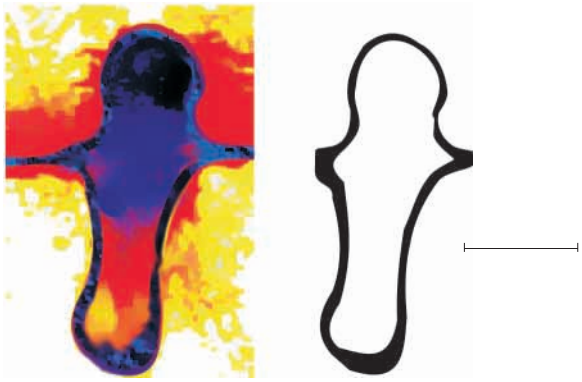

Fig. 3. (A) Original photograph of a section perpendicular to the long axis of an anal vein and the segmented vein walls. Scale bar, 0.1 mm. (B) The same image after editing to isolate the vein material from the background and conversion of the image to monochrome.

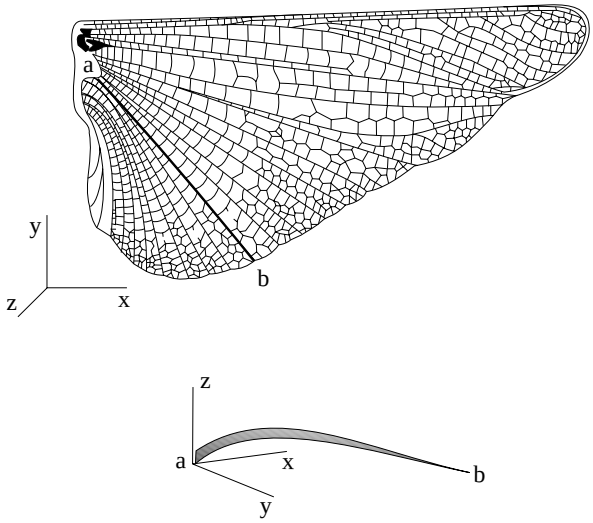

Fig. 4. The coordinate systems used to digitise the wing and vein profiles.

the wing deployed, leading to depression in the trailing edge (Fig. 6).

Finite element analysis

Model description

Five different finite element models of part of the vannus (anal fan) shown in Fig. 1 were generated using the commercial software package ANSYS 5.4.

Both the membrane and the dorsal longitudinal veins of the region shown in Fig. 1 were modelled, but the ventral veins and the small cross-veins were not included in the models. The ventral veins, positioned at the base of the wing corrugations, have much smaller cross-sectional areas and second moments of area than the dorsal veins, and therefore have much lower flexural rigidity. The purpose of the cross-veins within the context of wing deployment is unclear but, because their rigidity is very low, it was assumed that they contribute little to the mechanism being studied. The locust hind wing is always heavily corrugated at the leading edge, an adaptation to increase rigidity, even when fully deployed. This corrugation persists to produce some level of corrugation at the trailing edge, but its structural significance is much reduced. When the wing is deployed, the trailing-edge corrugation is less apparent and appears more as a series of ridges where the larger dorsal veins protrude from the membrane. When the trailing edge is depressed and the membrane is in tension, the corrugations flatten out almost completely. No corrugations were modelled, as a consequence of the omission of the ventral veins and because the initial or resting state of each model represented the point in deployment at which the membrane is taut and any corrugations are minimal.

The modulus of the membrane has been shown to range in the anal fan from 11.3 to 0.3 GPa (Smith et al., 2000). Although there was no clear pattern in the distribution of modulus, values closer to the margin were generally lower than those closer to the base of the wing. The membrane was divided into three bands (Fig. 6); the elements of the most proximal area were given a modulus of 5.1 GPa, those of the mid area 3.75 GPa and those of the most distal area 2.4 GPa, representing an average modulus within the three areas. The membrane material properties were assumed to be isotropic and to behave linear-elastically. The membrane was assumed to be of a constant 1.7 μm thickness (mean anal fan thickness in Smith et

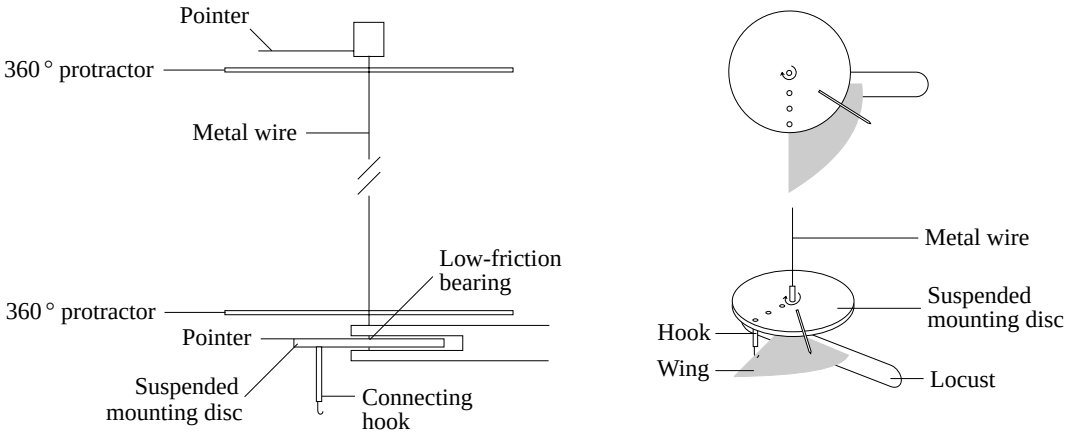

Fig. 5. The torsion balance used to extend the wing. The metal wire is manually rotated from the top, and the degree of rotation is read from the two 360 ° protractors. The two diagrams to the right show an isometric and top view of the mounting disc, illustrating how the wing was attached to the balance.

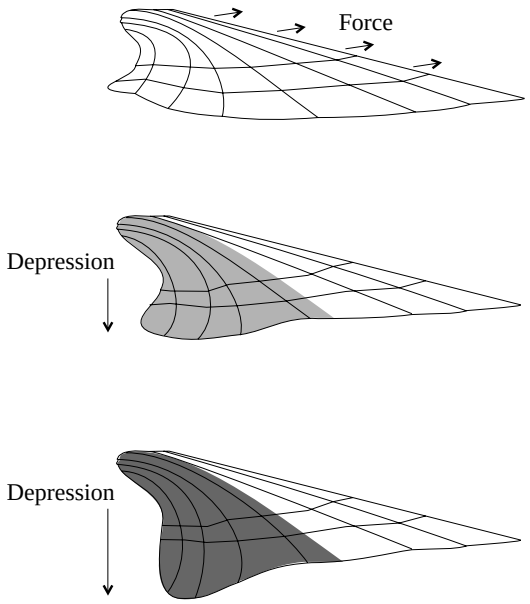

Fig. 6. The behaviour of a locust hind wing when deployed. As the leading edge is deployed, depression and camber generation occur in the wing, the greatest depression occurring in the posterior region of the anal fan. The division of the membrane into the three bands used in the model is indicated, as are the veins used in the model.

al., 2000) and was meshed with two-dimensional thin-shell elements.

The modulus of the vein material has not been directly measured, but published values for insect cuticle range from very stiff sclerotised cuticle at 9 GPa (Jensen and Weis-Fogh, 1962) in the locust tibia, which may represent the upper limit of stiffness in cuticle, to as low as 2×10^{-4} GPa in the softened cuticle of female locusts (Vincent, 1990). A modulus of 6 GPa was chosen for the vein material as representing an average value for published data concerning sclerotised cuticle. The vein material was assumed to be isotropic and to behave linear-elastically. The veins were meshed using three-dimensional elastic beam elements.

The details of the five models are as follows.

(i) The 'comprehensive' model. This is the most realistic model constructed. The model is based on the accurate digitised three-dimensional geometries (*x*, *y* and *z* coordinates) for the outline and vein placement, as shown in planform view in Fig. 7A. The model includes the pre-camber out-of-plane curvature of the vannus, and the tapered veins were approximated using a 'stepped beam' approach with a total of six uniform segments for each vein; values of second moments of area (I_{xx}, I_{yy} and I_{xy}) used for each segment were as obtained from the experimental measurements.

(ii) The 'no-camber' model (Fig. 7B). This model is based on the comprehensive model and is identical in all respects except that the initial curvature or camber of the wing is neglected, all the points on the wing are assumed to lie in the *xy* plane. In other words, the anal fan is assumed to be flat prior to applying the load.

(iii) The 'straight-veined' model (Fig. 7C). This model is again based on the comprehensive model, but now the curvature of the veins in the plane of the wing is neglected. The out-of plane curvature or initial pre-camber of the anal fan is, however, modelled.

(iv) The 'identical-vein' model (Fig. 7D). This model is identical to the comprehensive model except that the tapering of the veins is not modelled. Each vein is assumed to have values of the second moment of area that are constant along its length and equal to the values measured at the basal point of the leading edge vein (i.e. $I_{yy}=1.29\times10^{-4}$ mm^4, $I_{xx}=0.26\times10^{-4}$ mm^4, $I_{xy}=1.54\times10^{-4}$ mm^4).

(v) The 'mock-geometry' model (Fig. 7E). This model is constructed using geometry for the wing outline and vein placement approximated from the real wing. The purpose of this model is to show the effects of crudely approximating the shape of the wing and the arrangement of the veins. The veins are placed approximately the same distance apart from one another as in the real wing, but are joined at the top, the ano-jugal bar, by a straight line, rather than a curved structure as seen in the real wing. The curve of every vein is similar, and the membrane margin is simply a straight line between the tips of each vein. All veins are constructed using the second moments of area measured from the corresponding positions in the real wing. The model incorporates all measured material properties of the veins and membrane, but has a modified geometry.

Mesh generation

All five models were meshed using parabolic order elements because they include mid-side nodes that allow for elements with curved edges and a more accurate fit to the underlying geometry. A convergence test was performed by refining the mesh until further refinement resulted in no substantial change (<10 %) in the computed displacements of the anal fan under loading. For the 'comprehensive' model, a mesh consisting of 1669 elements (220 beam and 1449 membrane elements, Fig. 8) was found to give satisfactory results.

Boundary conditions

The veins were constrained at their base with only one rotational degree of freedom about the *x* axis. In reality, the veins are capable of rotating in all three directions *via* movements of the axillary muscles. As the axilla was not included in this model and the wing muscles were cut in the camber experiment, the degrees of freedom at the base of the model veins were reduced to one. The boundary conditions of the models assume that the veins cannot translate forwards or backwards relative to the body. Although the whole of the ano-jugal bar can be moved to some degree *in vivo*, this only occurs beyond the extension needed to generate camber.

Loads were applied to the most anterior vein of the anal fan as a uniformly distributed beam load. Although in the actual wing the load is applied at the base as a torque on the leading vein, this load would be transferred through the membrane to each vein, resulting in a distributed load on the leading vein of

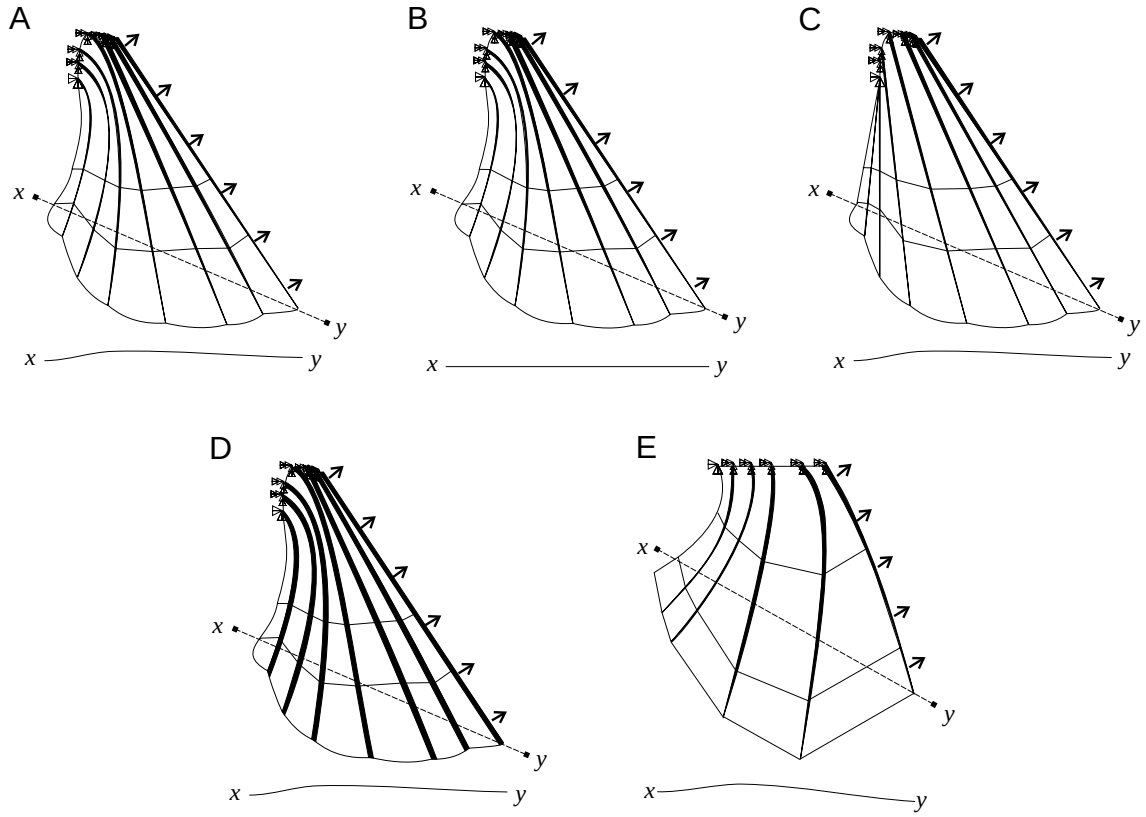

Fig. 7. The geometry, boundary and load conditions of the five finite element analyses. (A) The 'comprehensive' model; (B) the 'no-camber' model; (C) the 'straight-veined' model; (D) the 'identical-vein' model and (E) the 'mock-geometry' model. The tapering of the veins and the change in thickness between veins is indicated, except for the 'identical-vein' model whose veins all have identical cross sections. The lines dividing the membrane into three bands, each with a different modulus value, are also shown. The line below indicates the profile of each model, through points *x*–*y*. All models were restricted to zero translation at the base of the first vein, indicated by a single triangle, and pin joints at the base of all other veins, indicated by double triangles. The arrows indicate the direction of the distributed beam load.

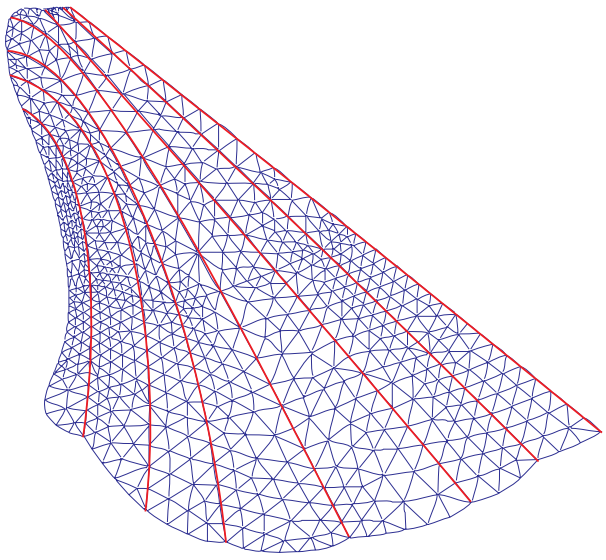

Fig. 8. The final mesh for the 'comprehensive' model consisting of 220 beam (red) and 1449 membrane (blue) elements.

the anal fan. As the model deformed, the load was always applied normal to the vein (follower force).

Model solution

Quasi-static loading was assumed (aerodynamic loads and inertial forces were ignored), and the model was solved allowing for large, non-linear deformations. Each model was subjected to sequential, distributed beam loads, from 0.002 N m, in increments of 0.002 N m, deploying the wing until, where possible, a total depression (and/or elevation) of between 0.9 and 1.1 cm was produced in the vannus. This was measured as the maximal point of translation in the *z* axis, and the computed torque required was compared with the torque measured in the camber test experiments.

Results

Vein structure and area moments

The changes along the veins from tip to base in the second moments of area about the neutral planes shown in Fig. 2 and the polar moment of area are shown in Fig. 9. In all the longitudinal veins examined, I_{xx} and I_{yy} decreased non-linearly

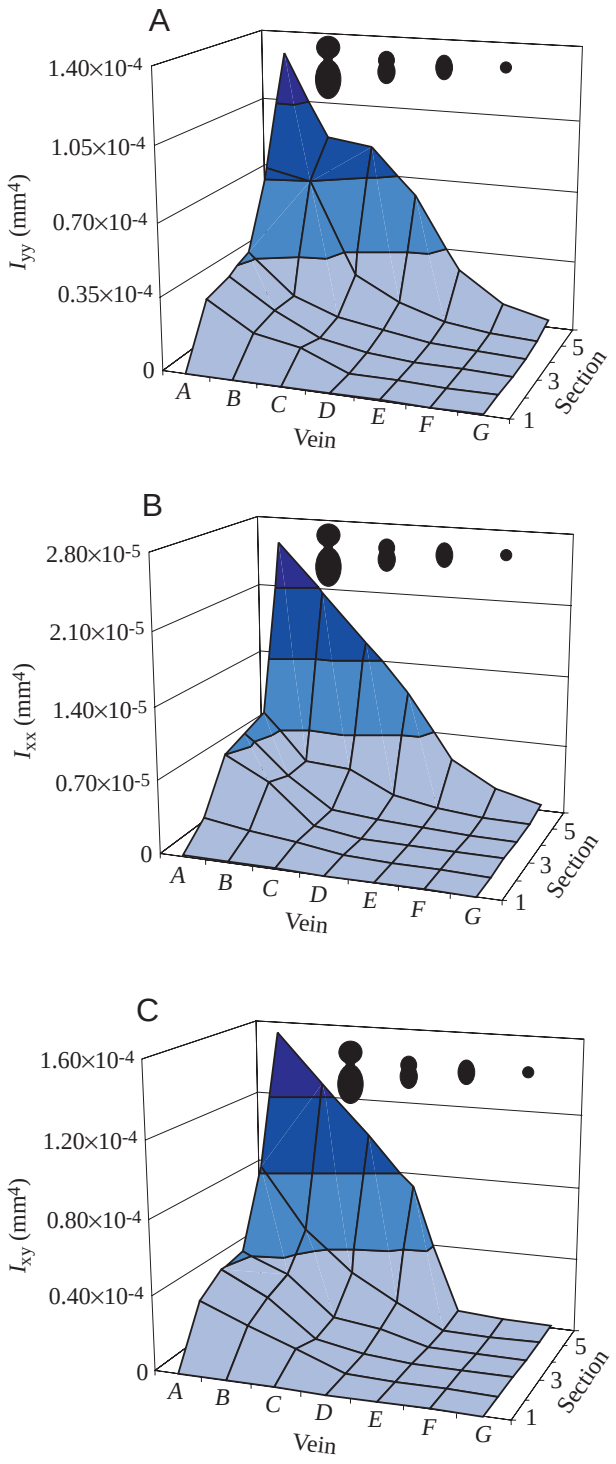

Fig. 9. The change in the three moments of area measured, I_{yy} (A), I_{xx} (B) and I_{xy} (C), along each vein, *A*–*G*, and each section, 1–6, the positions of which are shown in Fig. 1. The approximate shape of four sections along the most anterior vein is shown in black.

as the veins tapered from the base to the tip. I_{yy} for each vein section was consistently higher than I_{xx}, and the maximum I_{yy} value was nearly five times the maximum I_{xx} value. The torsional or polar moment of area is related to both I_{yy} and I_{xx} and, consequently, followed a similar pattern and extent.

Experimental tests

A mean torque of $9.4\times10^{-4}\pm1.3\times10^{-4}$ N m (mean ± S.D.) was required to deploy the locust hind wing fully. Previously conducted tests, using similar equipment, required opening torques of 9×10^{-4} N m to deploy complete hind wings from the closed position (Pitts, 1996; K. Pitts, personal communication). These results are very similar to our own, suggesting that the technique is robust.

The experimental torque required to depress the trailing edge by 1 cm when deploying the whole wing was $6.3\times10^{-5}\pm0.7\times10^{-5}$ N m. This decreased to $3.5\times10^{-6}\pm0.6\times10^{-6}$ N m when just the anal fan was isolated and deployed. In both the complete wing and the isolated vannus, depression and camber were generated long before the wing was fully extended. Crucially, while the whole outer margin was to some extent lowered, the greatest depression took place in the inner, postero-proximal part of the wing's trailing edge. Thus, as an in-plane force was applied to the leading edge of the wing or isolated vannus and the wing deployed, the umbrella effect caused depression in the anal fan. The area displaying the most depression was the very posterior portion of the vannus (Fig. 6). A plot of torque against deployment angle for a wing obtained with the same apparatus appears in Fig. 7 of Wootton et al. (2000).

Finite element models

The torques required to induce a 1 cm depression as computed using the five different finite element models of the anal fan are given in Table 1.

The closest value to the average experimentally measured torque of $3.5\times10^{-6}\pm0.6\times10^{-6}$ N m was obtained using the comprehensive finite element model (1.7×10^{-6} N m). The torque computed for the mock-geometry model was also reasonably close (1.2×10^{-6} N m). For both the identical-vein and the straight-veined models, computed torques (4.8×10^{-5} N m and 4.4×10^{-5} N m respectively) were an order of magnitude higher than the experimentally measured torque. The no-camber model failed to generate any depression under loading.

In Figs 10–14, the deformations of the five wing models under loading are plotted. Interestingly, only the comprehensive model produces deformations that are similar to those observed *in vivo* (Figs 10, 15). For all other models, qualitatively different deformations are produced under loading. For the mock-geometry model, the region with the largest depression is not the posterior, but the central portion of the wing margin (Fig. 11). For the straight-veined model (Fig. 12), the deformation is principally in the positive *z* axis (elevation), in contrast to the real wing (depression). The identical-vein model (Fig. 14) produces incorrect deformations, the mode of which alters according to the total applied load. At lower load levels (Fig. 14A), the point of maximum translation is towards the centre of the wing margin, but at higher loads (Fig. 14B), the leading edge becomes the maximum translation point. The no-camber model produces no

Table 1. *The loads and torques applied to each of the five models to produce approximately 1 cm of camber*

Model	Load applied to leading edge (N m)	Leading edge length (m)	Total load (N)	Mean torque (N m)
(i) Comprehensive	0.0060	0.022	0.00015	1.7×10^{-6}
(ii) No camber	–	–	–	–
(iii) Straight veined	0.1800	0.022	0.00400	4.4×10^{-5}
(iv) Identical vein	0.2000	0.022	0.00440	4.8×10^{-5}
(v) Mock geometry	0.0025	0.025	0.00005	1.2×10^{-6}

The no-camber model failed to produce any camber.

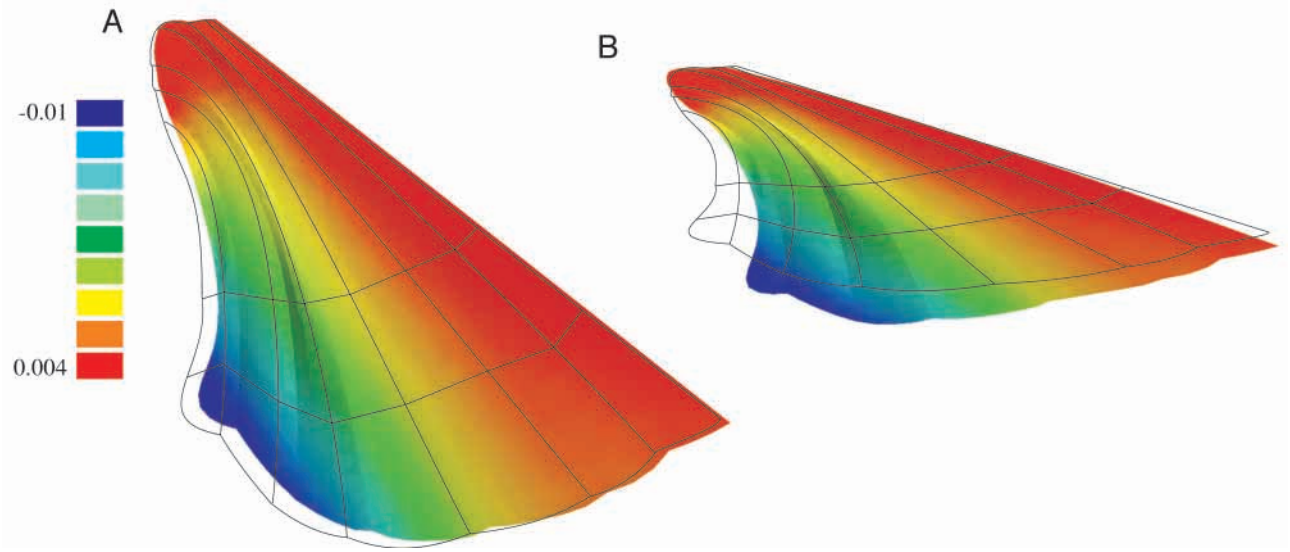

Fig. 10. The 'comprehensive' model subjected to a load of 0.006 N m. (A) Dorsal view and (B) latero-dorsal view; the colour represents translation in the *z* axis, either positive (elevation) or negative (depression) in metres. The black lines illustrate the undeformed shape of the wing.

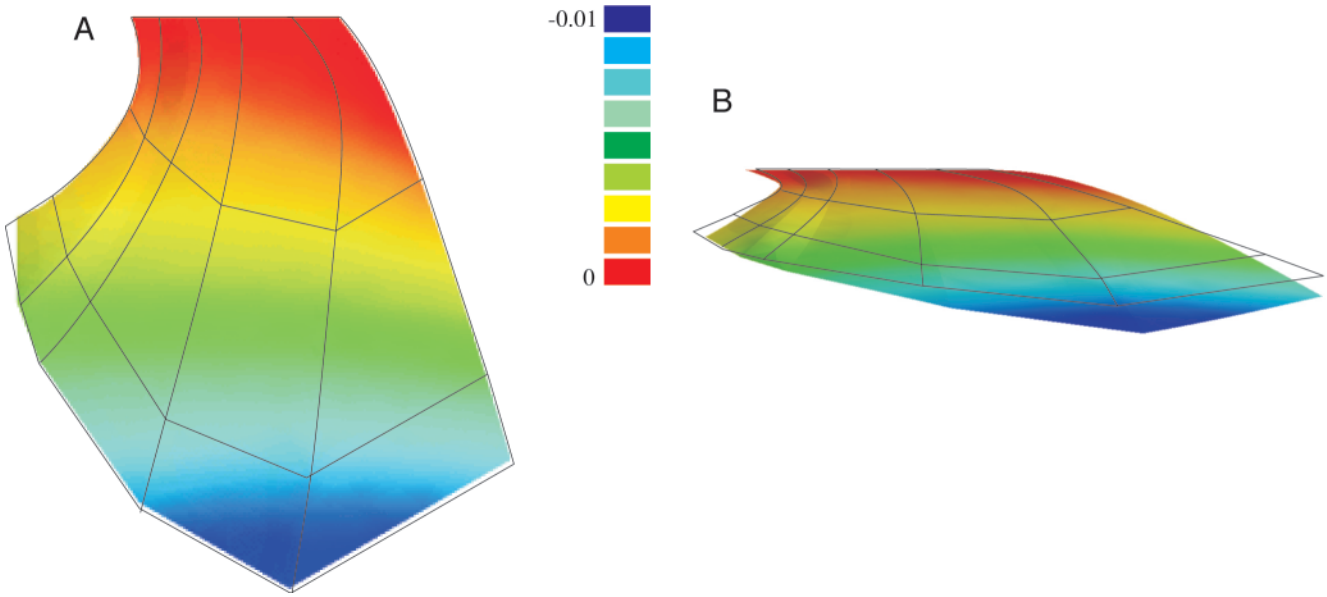

Fig. 11. The 'mock-geometry' model subjected to a load of 0.02 N m. (A) Dorsal view; (B) latero-dorsal view. The black lines illustrate the undeformed shape of the wing. The colours represent translation in the *z* axis in metres. Positive values indicate elevation; negative values indicate depression.

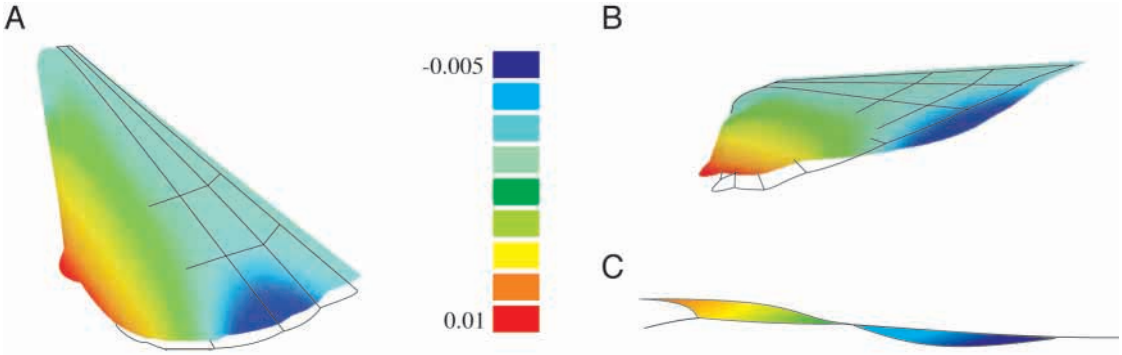

Fig. 12. The 'straight-veined' model subjected to a load of 0.0025 N m. (A) Dorsal view, (B) latero-dorsal view, (C) distal view. The black lines illustrate the undeformed shape of the wing. The colours represent translation in the *z* axis in metres. Positive values indicate elevation; negative values indicate depression.

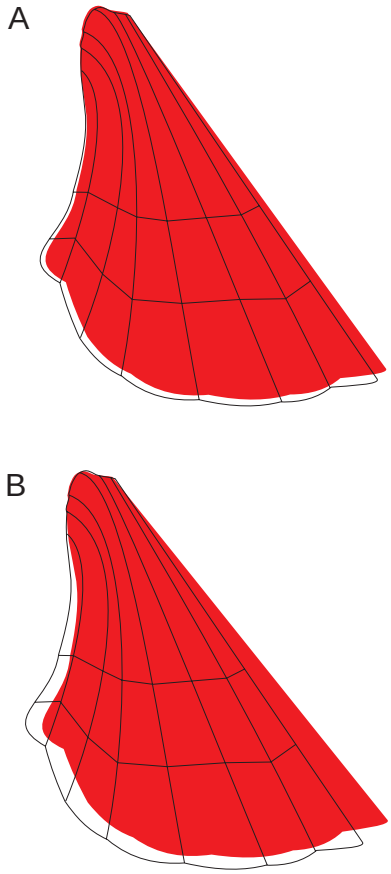

Fig. 13. The 'no-camber' model subjected to a load of 0.002 N m (A) and 5 N m (B). The black lines illustrate the undeformed shape of the wing. No translation in the *z* axis occurred.

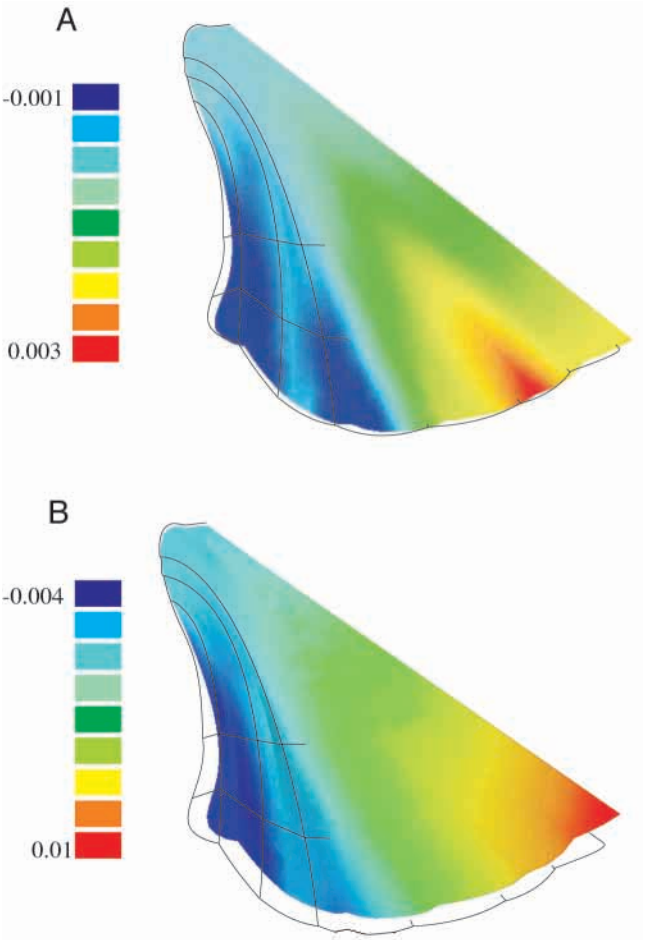

Fig. 14. The 'identical-vein' model subjected to a load of 0.065 N m (A) and 0.1 N m (B). The black lines illustrate the undeformed shape of the wing. The colours represent translation in the *z* axis in metres. Positive values indicate elevation; negative values indicate depression.

depression or elevation, and increases in applied force simply lead to a larger translation in the plane of the wing (Fig. 13).

In Fig. 15, the observed deformations of a locust wing in flight (Fig. 15A) are shown next to the numerically computed deformations of the comprehensive model (Fig. 15B). The camber is generated at similar angle in the trailing edge of the complete model as occurs in an actively flying locust.

Discussion

The observed tapering of the veins in the hind wing of the desert locust is, at least in part, a natural adaptation to structural loading. Indeed, the bending moments due to aerodynamic

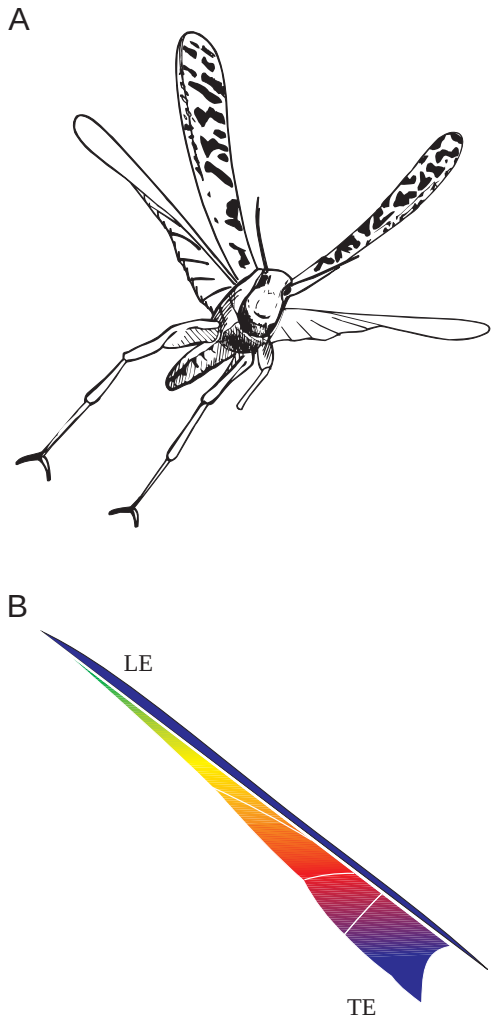

Fig. 15. (A) *Schistocerca gregaria* in free flight, illustrating the angle and amount of camber generated in the trailing edge. Traced from a photograph from Dalton (1975), with permission. (B) For comparison, the loaded 'comprehensive' model displaying a similar mode of deformation in the trailing edge (TE), with the leading edge (LE) at a similar angle.

loading of the wing will decrease from the ano-jugal bar to the wing margin, and the tapering of the veins will tend to minimise mass and moments of inertia for appropriate rigidity, which is important in oscillating structures and particularly so in a migratory species, where energy conservation is necessary. However, the form of the taper is highly non-linear and must also have a significant influence on the precise form of the camber generated by deployment.

The cross sections indicate that the veins are optimised for resisting bending moments about the neutral *x* axis, which is to be expected, because this will be the principal direction of loading. Fig. 3 clearly shows the asymmetry in the veins between the medio-lateral and dorso-ventral planes, which leads to the difference between I_{xx} and I_{yy}. The higher flexural rigidity about the neutral *x* axis is due to the elliptical hollow cross-sectional shape of the veins in which material is concentrated away from the neutral axis, thereby providing a high stiffness to mass ratio. It is not until close to the wing tip that the veins adopt a circular cross section, and the I_{xx} and I_{yy} values are equal. At this point, too, the differences in cross-sectional area and in moments of area between different veins are minimal. In the real wing, the cross-veins and the membrane prevent flexion of the veins about the neutral *y* axis.

The results obtained from the numerical simulation of deployment using the five finite element models were very different. Only the 'comprehensive' model produced deformations that matched both the experimental data on real wings under similar loading and the shape that wings assume in actual flight (Fig. 15). The other four models all failed to reproduce similar deformations to those of the actual wing despite having many similar characteristics. The torque required to produce a 1 cm depression in the trailing edge of the 'comprehensive' model was approximately half that obtained experimentally. This difference may be due the extra resistance of the cuticle of the axillae, to which the wing is still attached and which the model does not include.

The 'straight-veined' model produced two areas of high transition, both a depressed region and an elevated region. By forming straight lines between the point of origin of the veins and the wing margin, the relationship between the angle of the plane of vein cambering and the angle at which the margin exerts its force on the vein tips is increased. The curve of the veins in the real wing and the complete model enables the margin to exert a force that is more parallel with the plane of cambering. So, when a distributed load is applied through the wing margin, it is initiating Euler buckling more effectively by bending the vein closer to the plane in which camber already exists. In effect, by straightening the vein, some advantage of pre-cambering is lost. This effect is also likely to be occurring in the 'mock-geometry' model, in which the relative placement of the veins and the shape of the wing margin are altered.

The 'identical-vein' model produces a load-dependent deformation. The area of maximum translation moves round the wing margin anteriorly as the load is increased. As each vein in the model has identical stiffness, there is no reduction in overall stiffness from anterior to posterior veins. This has the effect of causing the anterior veins to buckle before the posterior ones. The most anterior vein may be prevented from buckling initially by the distributed load, but as the load is increased this vein also buckles, producing the final deformation.

The 'no-camber' model produces no depression in the trailing edge upon loading. The pre-cambering of the veins in the real wing (which was included in all other models) enables Euler buckling to occur smoothly along the length of the veins. Because the camber of the veins is in the same direction as the desired depression, a smooth transition from an unloaded to a loaded depressed state can be achieved. For the model without pre-cambering, the out-of-plane buckling behaviour will not occur smoothly. A cardboard model consisting of radiating flat spokes, restrained at their tips by cord, illustrates this well. When the force is applied carefully, the model will tend to snap to either an elevated or a depressed state as the model passes

through a singularity. Once the spokes have been buckled, the depression or elevation will continue smoothly.

These results suggest that the wing shape, as well as the properties of the veins and membrane, is structurally very significant. The range of deformations produced by subtly altered models emphasises the degree of design integration that one finds in biological structures. If man-made structures are eventually to emulate automated, passive biological structures, an integrated design philosophy may well be essential.

The finite element method was born of engineering principles and is still used mainly in engineering. The materials used and the loading patterns encountered are generally much better appreciated in the analysis of human-engineered structures. It is common practise to create an optimised simple model and only include limited complexities, and these models often provide sufficient information.

The range of structural responses to loading obtained using the approximate numerical models presented here clearly demonstrates how much more complexity is required in this biological case to achieve accurate results. The vein shape, vein size, vein position and wing shape interact intimately with one another to produce the observed deformation, and over-simplifying any of these caused the model to fail even at the basic level of qualitatively reproducing observed deformations. Not only was a surprisingly sophisticated model required to give reasonably accurate results, but also the response of the model was very sensitive to minor simplifications. These results serve to highlight the need to validate every simplification of a model before it can be accepted.

Only a small portion of the hind wing was included in the model. Increasing the scope of the model to include the whole wing, its corrugations and some of the axillae would enable more accurate load and boundary conditions to be applied. Sensitivity analysis should be applied to the model to gauge the sensitivity of the deformation to the parameters of material stiffness and the shape of the veins and to evaluate the relative importance of the features discussed here.

This research was carried out with the assistance of BBSRC Special Studentship 3178 and BBSRC grant SO7722.

References

Argyris, J. H. (1965). Continua and discontinua. *Proceedings of a Conference on Matrix Methods in Structural Mechanics* (ed. A. F. B. Wright-Patterson), pp. 11–89. Ohio: Wright-Patterson A.F.B.

Cloupeau, M., Devillers, J. F. and Devezeaux, D. (1979). Direct measurements of instantaneous lift in desert locust; comparison with Jensen's experiments on detached wings. *J. Exp. Biol.* **80**, 1–15.

Courant, R. (1943). Variational methods for the solution of problems of equilibrium and vibrations. *Bull. Am. Math. Soc.* **49**, 1–23.

Dalstra, M., Huiskes, R. and Vanerning, L. (1995). Development and validation of a 3-dimensional finite-element model of the pelvic bone. *J. Biomech. Eng. Trans. ASME* **117**, 272–278.

Dalton, S. (1975). *Borne on the Wind.* London: Chatto & Windus.

Guldberg, R. E., Hollister, S. J. and Charras, G. T. (1998). The accuracy of digital image-based finite element models. *J. Biomech. Eng. Trans. ASME* **120**, 289–295.

Hirschberg, J., Milne, N. and Oxnard, C. E. (1999). Stresses, strains and adaptive remodelling in trabecular bone: a finite element approach. *Am. J. Phys. Anthropol.* **S28**, 153–159.

Huiskes, R. and Chao, E. Y. S. (1983). A survey of finite-element analysis in orthopedic biomechanics – the 1st decade. *J. Biomech.* **16**, 385.

Jensen, M. (1956). Biology and physics of locust flight. III. The aerodynamics of locust flight. *Phil. Trans. R. Soc. Lond. B* **239**, 511–552.

Jensen, M. and Weis-Fogh, T. (1962). Mechanical properties of locust cuticle. *Phil. Trans. R. Soc. Lond. B* **245**, 137–162.

Kesel, A. B., Philippi, U. and Nachtigall, W. (1998). Biomechanical aspects of the insect wing: an analysis using the finite element method. *Comput. Biol. Med.* **28**, 423–437.

Pitts, K. (1996). The morphology and mechanical properties of orthopteroid and dictyopteroid hind wing fans in relation to the mechanics of the *umbrella effect*. MSc thesis, University of Exeter.

Prendergast, P. J. (1997). Finite element models in tissue mechanics and orthopaedic implant design. *Clin. Biomech.* **12**, 343–366.

Prendergast, P. J. and Huiskes, R. (1996a). Microdamage and osteocyte-lacuna strain in bone: A microstructural finite element analysis. *J. Biomech. Eng. Trans. ASME* **118**, 240–246.

Prendergast, P. J. and Huiskes, R. (1996b). Finite element analysis of fibrous tissue morphogenesis – A study of the osteogenic index with a biphasic approach. *Mech. Composite Mat.* **32**, 144–150.

Smith, C. W., Herbert, R. H., Wootton, R. J. and Evans, K. E. (2000). The hind wing of the desert locust (*Schistocerca gregaria* Forskål). II. Mechanical properties and functioning of the membrane. *J. Exp. Biol.* **203**, 2933–2943.

Smith, T. S., Martin, R. B., Hubbard, M. and Bay, B. K. (1997). Surface remodeling of trabecular bone using a tissue level model. *J. Orthop. Res.* **15**, 593–600.

Snodgrass, R. E. (1925). *Principles of Insect Morphology*. London: McGraw-Hill.

Vincent, J. F. V. (1990). Composites. In *Biomechanics: A Practical Approach* (ed. J. F. V. Vincent), pp. 57–74. Oxford: Oxford University Press.

Watanabe, H. (1995). *Structural Analysis of Dragonfly Wings with FEM*. Tokyo: Kawachi Millibioflight Project Workshop.

Weis-Fogh, T. (1956). Biology and physics of locust flight. II. Flight performance of the desert locust (*Schistocerca gregaria*). *Phil. Trans. R. Soc. Lond. B* **239**, 459–510.

Weis-Fogh, T. and Jensen, M. (1956). Biology and physics of locust flight. I. Basic principles of insect flight: a critical review. *Phil. Trans. R. Soc. Lond. B* **239**, 415–458.

Wootton, R. J. (1992). Functional morphology of insect wings. *Annu. Rev. Entomol.* **37**, 113–140.

Wootton, R. J. (1993). Leading edge section and asymmetric twisting in the wings of flying butterflies (Insecta, Papilionoidea). *J. Exp. Biol.* **180**, 105–117.

Wootton, R. J. (1995). Geometry and mechanics of insect hind wing fans – a modelling approach. *Proc. R. Soc. Lond. B* **262**, 181–187.

Wootton, R. J., Evans, K. E., Herbert, R. C. and Smith, C. W. (2000). The hind wing of the desert locust (*Schistocerca gregaria* Forskål). I. Functional morphology and mode of operation. *J. Exp. Biol.* **203**, 2921–2931.

Young, W. C. (1989). *Roark's Formulas for Stress and Strain*, 6th edition. New York, London: McGraw-Hill Book Co.